

Article

Magnetic Characterization of the Nugget Microstructure at Resistance Spot Welding

Christian Mathiszik ^{*}, Edwin Zschetzsche, André Reinke, Johannes Koal , Jörg Zschetzsche and Uwe Füssel

Institute of Manufacturing Science and Engineering, Chair of Joining Technology and Assembly, Technische Universität Dresden, 01069 Dresden, Germany

* Correspondence: christian.mathiszik@tu-dresden.de; Tel.: +49-351-463-34346

Abstract: Conventional resistance spot welds are not visible from the outside. Therefore, it is not straightforward to evaluate the joint quality non-destructively. The pulse-echo method of manual ultrasonic is widely used for non-destructive testing. Another option is the passive magnetic flux density testing, which is being developed at Technische Universität Dresden, Germany. The spot weld is magnetized in the normal direction and the residual magnetic flux density is measured on top of the surface of the joint. This method is suitable for spot welds on typical car body steels. Previous investigations show that the magnetic properties of the materials influence the test result. In order to develop this new non-destructive testing method further, it is necessary to know the magnetic properties of the different microstructure regions of a spot weld. This article focuses on methods to measure and evaluate the magnetic properties of these regions, especially of the base material and the weld. Different measuring methods and approaches are presented and compared with each other. Based on the results, recommendations for future measurements for magnetic characterizations are given.

Keywords: resistance spot welding; magnetic material characterization; ferromagnetic steel; non-destructive testing; nugget structure; hysteresis loops; residual magnetic flux density; vibrating sample magnetometer



Citation: Mathiszik, C.; Zschetzsche, E.; Reinke, A.; Koal, J.; Zschetzsche, J.; Füssel, U. Magnetic Characterization of the Nugget Microstructure at Resistance Spot Welding. *Crystals* **2022**, *12*, 1512. <https://doi.org/10.3390/cryst12111512>

Academic Editors: Benjamin Strass, Susann Hausner and Cyril Cayron

Received: 27 September 2022

Accepted: 21 October 2022

Published: 25 October 2022

Publisher's Note: MDPI stays neutral with regard to jurisdictional claims in published maps and institutional affiliations.



Copyright: © 2022 by the authors. Licensee MDPI, Basel, Switzerland. This article is an open access article distributed under the terms and conditions of the Creative Commons Attribution (CC BY) license (<https://creativecommons.org/licenses/by/4.0/>).

1. Introduction

Resistance spot welding (RSW) is a widely used welding process in the sheet metal processing industry. This includes mechanical and plant engineering, equipment technology and body-in-white constructions. In the latter, the highest quality and safety requirements are imposed in conjunction with an enormously high number of spot welds. The challenge for quality assurance is the concealed position of the spot weld between the sheets. A schematic representation of a spot-welded joint with the most important geometric parameters and microstructural regions is shown in Figure 1.

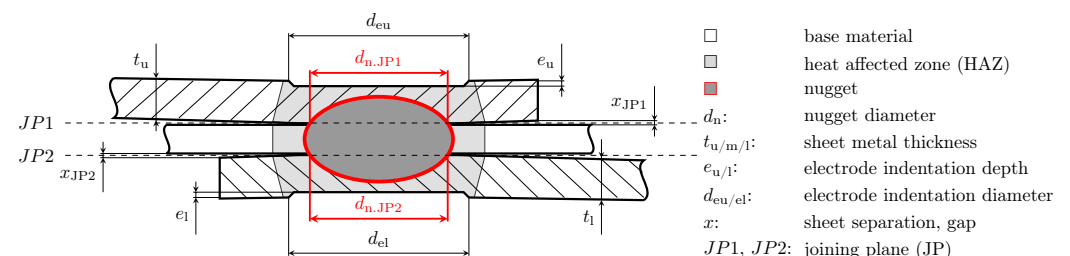


Figure 1. Schematic illustration of a spot-welded joint with three sheets and the main geometrical parameters with the highlighted nugget diameter d_n as the most important one.

These geometric parameters can be divided into those that are visible from the outside and those that are not. The weld diameter d_w and nugget diameter d_n are the most

important geometric evaluation parameters of a spot weld for quality assurance. Both diameters are not visible from the outside. This represents a major challenge for non-destructive evaluation of resistance spot welds.

The technical bulletin DVS 2916-5 [1] provides a good overview of the current possible non-destructive testing (NDT) procedures for RSW. It shows that manual ultrasonic testing using the pulse-echo method has been the most suitable method in the industrial environment to date. The imaging ultrasonic inspection systems with piezoelectric matrix- and phased-array transducers are currently gaining large acceptance. These systems usually determine the nugget diameter d_n and the electrode indentation depth $e_{u/1}$ for the evaluation of the spot-welds. Another option for NDT of the welded joint is passive magnetic flux density testing (pMFT). This method is developed at Technische Universität Dresden, Germany, and is currently being further investigated scientifically [2–6]. The spot weld is magnetized in the normal direction and the residual magnetic flux density at the surface is measured afterwards. The measurement is performed by scanning with a single Hall-sensor or with a Hall-sensor-array. The measured magnetic field distribution is evaluated and the weld area is determined for quality assessment. The testing procedure is shown in Figure 2.

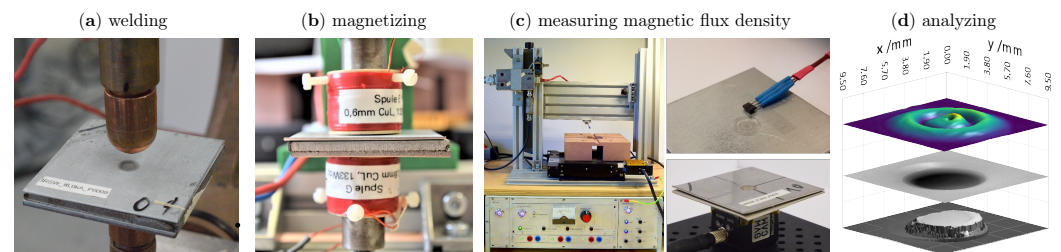


Figure 2. Test sequence for the passive magnetic flux density testing (pMFT) with (a) RSW-process, (b) magnetizing the spot weld with two coils oriented in the same direction, (c) measuring the residual magnetic flux density on the surface of the samples by scanning with one Hall-sensor (left and upper image) or by a Hall-sensor-array as a magnetic field camera MiniCube 1D provided by MAGCAM (lower image), and (d) analyzing the measured data with correlation to the nugget size of the spot weld.

Investigations in [2–6] show that this new NDT-method is suitable for the quality evaluation of spot-welds with material combinations that are typical for RSW. It was found that the test results depend on the geometrical conditions of the spot weld and on the welded material. In the case of the geometrical conditions, the electrode indentation parameters ($e_{u/1}$, $d_{eu/el}$) and the weld area are decisive. In [7] it was shown that the electrode indentation plays a subordinate role as long as it is within the limits of the standardized permissible depth of $e_{max} \leq 20\%$ regarding the thinner sheet within the material combination according to ISO 14373 [8]. With regard to the influence of the material, it was shown in [9] that spot welds of the austenitic steel X5CrNi18-10 (1.4301) can also be tested. This steel has no ferromagnetic properties as base material and it shows no magnetic behavior. However, the microstructure of the nugget exhibits ferromagnetic properties. The reason for this is the high cooling rates of more than 1000 K s^{-1} where delta ferrite remains and can be detected inside the nugget. Delta ferrite has ferromagnetic properties. Thus, after magnetization of the spot weld, the residual magnetic flux density of the nugget can be measured and the joint can be evaluated non-destructively. These investigations indicate that the magnetic properties of the different structural regions of the weld influence the test results. These regions include the base material, the heat-affected zone (HAZ) and the nugget. The purpose of this article is to present the results of investigations dealing with the characterization of magnetic properties of the different regions of spot-welded joints of different steel alloys. Promising measuring methods are presented and compared with each other. The results provide the basis for further developments of the new NDT-method pMFT.

2. Brief Fundamentals of Measuring Magnetic Material Properties

According to their magnetic behavior, materials can be classified into those with ferro-, antiferro-, ferri-, para- and diamagnetic properties [10]. In this article, the ferromagnetic behavior of the investigated materials is of particular interest, since weld microstructures usually exhibit ferromagnetic behavior. This depends, among other things, on their alloy composition. One possible way of describing the magnetic properties is the flux density—field strength diagram (B - H -diagram). The following characteristic values can be taken from the B - H -diagram:

- Residual magnetic flux density B_r : Magnetic flux density that remains in the material when no external magnetic field is applied after previous magnetization;
- Coercivity H_c : magnetic field strength necessary to obtain a magnetic flux of $B = 0$ (with previous magnetization);
- Magnetic saturation H_s, B_s : point beyond which a change in magnetic field strength causes only a small change in flux density.

The area enclosed by the curve is a measure of the energy required for remagnetization. The larger the area, the more energy is required and vice versa [11]. Ferromagnetic materials can be divided into hard and soft magnetic materials. The classification is made according to the level of coercivity H_c . Materials with a high coercivity ($H_c > 1000 \text{ A m}^{-1}$) are considered magnetically hard [12]. An application example of hard magnetic materials are permanent magnets. One application of soft magnetic materials is the construction of transformer cores. In the range of coercivity H_c , μ_r is very large (e.g., iron: $\mu_r = 1000$ [13]), the residual magnetic flux density is small compared to hard magnetic materials. The area enclosed by the hysteresis loop is small, which means that less energy is required to remagnetize.

In a vacuum, H and B are linear related to each other by the magnetic field constant μ_0 (Equation (1)). If material is in a magnetic field, the relation remains, but the magnitude of the proportionality factor changes. This is called permeability μ and is the product of μ_0 and the relative permeability of the material μ_r (Equation (2)). μ_r depends on the material. Another parameter is the magnetic polarization J , which is defined as the difference between the flux density in vacuum and the measured flux density at a certain field strength (Equation (3)) and describes the intensity of the magnetization [13]. For ferromagnetic materials the relationship between H and B results in a characteristic magnetic hysteresis loop, as shown in Figure 3. In general, the fully saturated hysteresis loop (H -loop) is determined for this purpose. The main magnetic hysteresis loop and the initial magnetization curve show a characteristic curve for each material, which can be mainly defined by the saturation, the residual magnetic flux density B_r , the coercivity H_c and the Rayleigh constant α_R [14]. In addition to the main hysteresis loop, smaller loops can also be determined, which always lie within the main loop. These loops are called Rayleigh loops (R -loops) according to *Lord Rayleigh*, as described in [15]. The reversal points lie on the commutation curve, which corresponds to the positive and negative initial magnetization curve [14]. As can be seen in Figure 3, the magnetization depends on the magnetic history of the material. The Rayleigh loops show that the residual magnetic flux density B_r also depends on the applied magnetic field strength H . Since the pMFT-method is based on the measurement of the residual flux density of the spot welds and no homogeneous magnetization of these is possible, the dependence of the residual flux density and the generated magnetic field is one focus of this article.

$$B = \mu H \quad (1)$$

$$\mu = \mu_r \mu_0 \quad (2)$$

$$J = B - \mu_0 H. \quad (3)$$

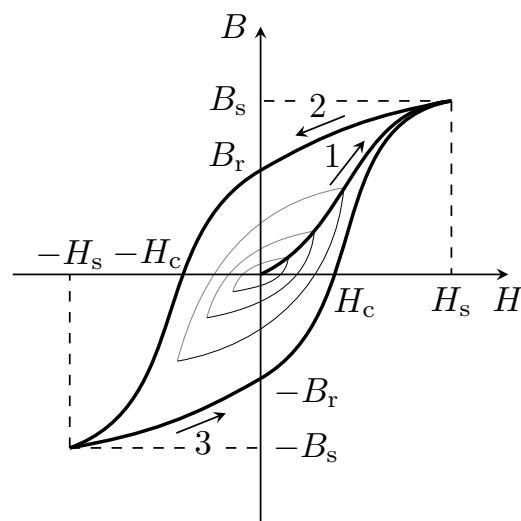


Figure 3. Schematic illustration of a hysteresis loop with the initial magnetization curve (1), upper hysteresis curve (2), lower hysteresis curve (3), the saturation points $\pm H_s$, $\pm B_s$ and the characteristic magnetic parameters coercivity H_c and residual magnetic flux density B_r of the main loop and three inner Rayleigh loops.

3. Preliminary Studies

In a first experimental setup, measurements are performed on cross-section samples of the steel alloy HX340LAD (MAT2, Table 1). The cross-section samples are magnetized with a magnetization current up to $I_{\text{mag}} = 35$ A using two magnetization coils oriented in the same direction. The residual magnetic flux density is measured at the surface of the cross-section. The aim of the measurements is to provide basic evidence that the weld has different magnetic properties than the base material. Based on these experiments, the materials and methods for the followed examinations are planned.

Table 1. Investigated materials with microstructure of the base material and magnetic behavior in the delivery condition.

ID	Material	Microstructure Base Material	Magnetic Behavior
MAT1	22MnB5 (1.5528)	martensite	ferromagnetic
MAT2	HX340LAD (1.0933)	ferrite	ferromagnetic
MAT3	X5CrNi18-10 (1.4301)	austenite	non-ferromagnetic
MAT4	S235 (1.0038)	ferrite	ferromagnetic

4. Materials and Methods

4.1. Investigated Materials

Since RSW is widely used in the automotive car body manufacturing combined with the highest safety requirements, the material selection is based on currently used steel alloys in this field (MAT1, MAT2). Additionally two commonly used steel alloys in civil engineering (MAT3, MAT4) are also investigated. The selected materials and their magnetic behavior in normal and conventional delivery condition are listed in Table 1.

4.2. Selected Methods for Measuring the Magnetic Material Properties, Sample Preparation and Geometries

The results of the preliminary studies in Section 5.1 show that it is important to measure the magnetic properties on the unaffected microstructure of the weld. Different measuring principles can be used to determine the hysteresis loops. Based on DIN EN 60404-4 [16], measurements are often performed on toroidal samples with one excitation and one measuring coil. These offer the advantage of a closed magnetic circuit [17]. For the

weld specimens considered in the article, this method can be used for the base materials, which are available as sheets. These investigations were already carried out as part of the development of the pMFT-method in the research project IGF 19.208 BR [5] with the support of the company *Ilmenauer Mechatronik GmbH*. Here, rings of the base material are cut out of the sheets by water jet cutting to reduce the temperature influence. For the toroidal core, several rings are stacked on top of each other and wrapped with copper enamel wire for the excitation and measurement coils. For this article, the measurement results are reprocessed to characterize the base materials in terms of their magnetic behavior. This particularly affects a recalculation of the magnetic field strength H . The hysteresis loops for the toroidal samples are calculated by Equations (4) and (5). N_1 and N_2 are the numbers of windings of the primary and secondary coils. l_m is the average length of the rings. A_{cs} is the total cross-sectional area of the stacked rings and U_{ind} is the induced electric voltage of the secondary coil. The average length l_m can be calculated according to [16] by Equation (6). A better approximated is given by Equation (7) according to [11,18]. For the samples used, the differences of the two equations range from 0.67% to 0.7%. The geometric parameters of the toroidal cores are listed in Table 2. The number of the excitation coil windings is $N_1 = 300$ and for the measurement coil $N_2 = 150$. The magnetizing current was regulated up to $I_{mag} = \pm 10$ A.

$$H = \frac{N_1 I_{mag}}{l_m} \quad (4)$$

$$B = \frac{1}{N_2 A_{cs}} \int_{t_0}^{t_1} U_{ind} dt \quad (5)$$

$$l_m = \frac{\pi}{2} d_i + d_o \quad (6)$$

$$l_{m.Chang} = \pi \frac{d_o - d_i}{\ln d_o - \ln d_i} \quad (7)$$

Table 2. Geometries of the toroidal ring samples.

ID	Material	d_i /mm	d_o /mm	h /mm	l_m /mm	$l_{m.Chang}$ /mm	A_{cs} /mm ²
MAT1	22MnB5	29.88	39.9	9.18	109.61	108.85	45.99
MAT2	HX340LAD	29.93	39.85	9.7	109.61	108.86	48.11
MAT3	X5CrNi18-10	30	39.88	9.8	109.76	109.03	47.91
MAT4	S235	29.95	39.9	9.4	109.72	108.97	46.76

The use of an Epstein frame was also considered, but was discarded due to the additional expense of setting up the test rig according to the standard DIN EN 60404-2 [19], as there was no prospect of measuring the residual magnetic flux density of the weld. In [20], minor hysteresis loops or Rayleigh loops, respectively, of cold rolled steel were measured, but the experimental setup is not described in detail to adapt it to the requirements of this paper. However, the three methods described above cannot be used to determine the magnetic characteristics of the weld structure of the nuggets because they have a very small volume and, e.g., no rings can be cut out easily. In this case, the vibrating sample magnetometer (VSM) can be used. The geometric dimensions of the samples were in the range of typical nuggets, which usually do not exceed a diameter of 10 mm. Besides the usage of a VSM, an investigation method directly related to the pMFT-method described above for the NDT of spot welds was selected as residual magnetic flux density (RMFD).

For both methods, weld specimens were produced by RSW. For the VSM-measurements, two sheets were welded were used for each sample. The aim was to produce weld nuggets with a large volume. The welding parameters used are summarized in Table 3. A detailed description of the welding test rig can be found in [21]. Table 4 shows the data and values obtained from each method for further evaluations and the used sample geometries.

Table 3. Welding parameters used to produce the samples for the methods VSM and RMFD.

Material	Sheet Thickness t	Welding Current I_w	Welding Time t_w	Electrode Force F_{el}	Measuring Method
MAT1 ¹	2 × 1 mm	9.0 kA	360 ms	3.5 kN	VSM
MAT2 ¹	2 × 1 mm	9.0 kA	300 ms	2.7 kN	VSM
MAT1–MAT4 ²	3 × 2 mm	16.0 kA	1000 ms	3.6 kN	RMFD

Used electrode caps: ¹ ISO 5821 F1-16-20-40-6; ² ISO 5821 C0-16-20.

Table 4. Selected methods for measuring the magnetic material properties by the obtained values and sample geometries (third dimension depends on sheet metal thickness).

Method	Measured Values	Sample Geometry	Sample Dimensions
VSM	H-loop: H_c, H_s, B_s, B_r	Cuboid	2 mm × 6 mm
RMFD	Residual magnetic flux density B_r	Disc	$d = 25$ mm

For the investigations with the VSM and RMFD, the specimens were cut out by electrical discharge machining (EDM)-processes. They offer the advantages of only a very slight temperature effect and no mechanical changes to the weld structure were to be expected. The VSM-samples were cuboids as listed with the individual experimental conditions of the samples in Table 5. For each run, several samples were stacked. To expose the microstructure of the weld for the RMFD investigations, the outer sheets of the specimens were cut off by sinker EDM. Then, circular discs with a diameter of about $d = 25$ mm around the weld were cut out by wire EDM. Subsequently, the specimen discs were ground and polished under continuous water-cooling to produce a smooth surface. The specimens contained the microstructures of the base materials, the HAZ and the weld as separate and homogeneous volumes throughout the cross-section of the sample. In order to evaluate the geometric properties of the discs, topographic measurements were performed using a chromatic-confocal microscope (CCM).

Table 5. Individual geometries of the samples for the VSM-measurements.

Material-ID	Temperature	Mass	Volume	Number of Samples
MAT1, base material	25 °C	0.56 g	74.1 mm ³	6
MAT1, weld	25 °C	0.73 g	94.8 mm ³	8
MAT2, base material	25 °C	0.31 g	54.4 mm ³	5
MAT2, weld	25 °C	0.81 g	90.0 mm ³	8

4.3. Experimental Setup

The test rigs of the *Chair of Material Technology of Technische Universität Dresden* were used for the VSM-measurements. The RMFD-measurements were carried out with five specimen discs per material according to Table 4. The experimental procedure was similar to that of the pMFT shown in Figure 2. The coil configurations for the experimental setup were based on [2,5]. The publications showed that some materials were evaluated better with coils with ferromagnetic steel cores and others with air core coils. Due to limited accessibility, it may also be the case that only one side can be magnetized. The experimental setups for magnetizing the samples of Table 6 were intended to reflect the above variants. Therefore, a modular test rig was developed, which can be individually assembled according to the requirements. A schematic illustration is shown in Figure 4. The power source (1) and the measurement unit (2) were used in every test setup. To measure the magnetization current I_{mag} and voltage U_{mag} the measurement unit (2) was used. This module was also equipped with a solid-state relay controlled by an Arduino micro-controller through a digital interface (DI). This allowed the circuit to be interrupted in a time-controlled and event-based manner. This prevented the coils from overheating or burning out. The experi-

ments were performed with either two coaxial coils connected in series and oriented in the same direction on each side of the specimen (5) or with just one coil beneath the sample (5). Additionally the coil core material could be changed.

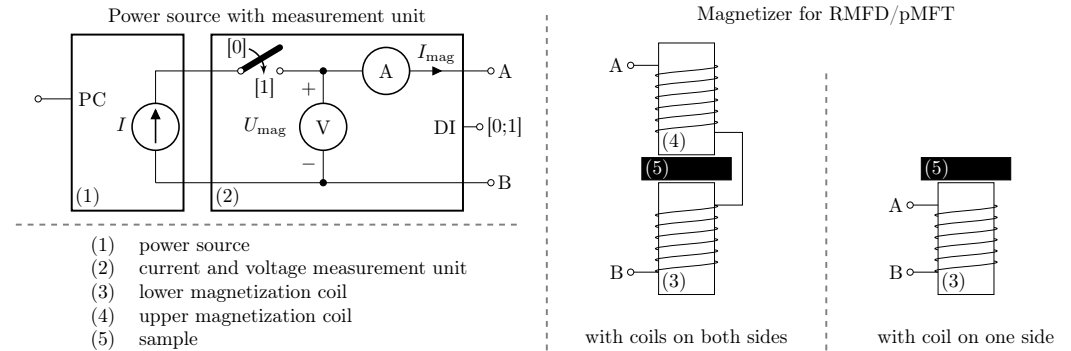


Figure 4. Schematic illustration of the modular developed test rig for measuring the magnetic properties of the materials and the welds.

Figure 5 shows the experimental setups. The discs (5) were placed directly on top of the lower coil (3). When using the upper coil (4), it was positioned directly on the upper specimen surface as shown in Figure 4. All samples were demagnetized prior to the experiments. Then each sample was magnetized gradually by an increasing magnetizing current $I_{mag} = 0\text{ A}, 5\text{ A}, 10\text{ A}, 15\text{ A},$ and 20 A . 1 A was additionally used for the air coil configurations. After each magnetization step, the vector component in z-direction of the residual magnetic flux density $B_{r,z}$ was measured with a Hall-probe at a distance of $z = 0.1\text{ mm}$ to the sample surface, which faced the lower coil. The scanning step size in x- and y-direction was 0.5 mm. The Hall-probe is a commercially available Hall-sensor of Allegro Systems A1324 UA with a measuring range of $\pm 50\text{ mT}$ and a sensitivity of 0.5 mV/mT . The sensor was connected to the measuring system via an amplifier with a gain of 3.0 and could be adjusted against external magnetic fields.

Table 6. Experimental configurations and parameters for measuring the residual magnetic flux density of the disc.

ID	Coil Configuration	Coil Core Material and Diameter
S1	1 coil D25, N180, one sided	steel 42CrMo4 (1.7225), $d = 25\text{ mm}$
S2	2 coils D25, N180, both sided, same oriented	steel 42CrMo4 (1.7225), $d = 25\text{ mm}$
A1	1 coil D25, N180, one sided	air, $d = 25\text{ mm}$
A2	2 coils D25, N180, both sided, same oriented	air, $d = 25\text{ mm}$

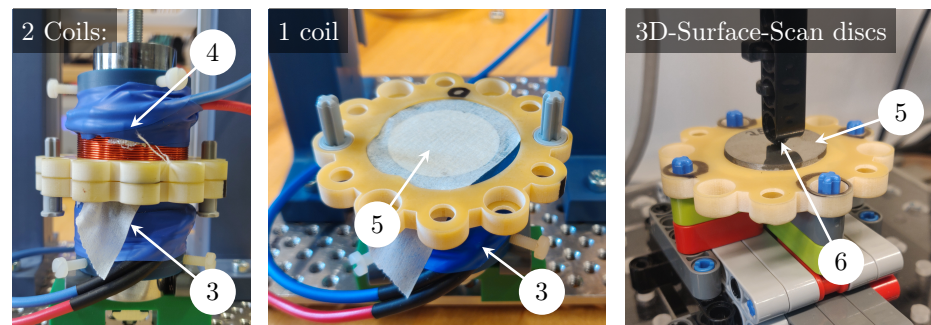


Figure 5. Magnetization modules for the disc samples with two coils (3,4) and the sample (5) in-between (left), one coil (3) with the sample (5) on top of it fixed with a piece of tape (middle) and the 3D-Surface-Scanner for measuring the residual magnetic flux density on top of the discs (5) with a single Hall-probe (6).

Prior to the RMFD-investigations, the magnetic flux density of the coil without a core was measured to validate the generated magnetic field. For this purpose, the Hall-probe was first passed through the air coil from bottom to top. The coil currents were set to 1 A and 2 A. In a second measurement, the magnetic flux density was measured above the coil with a coil current of 1 A. The step size in the axial direction (z) is $z = 0.5$ mm in each case. The measured values were compared with theoretical values according to the approximation Equation (8) of [22,23]. The magnetic field strength can then be calculated using Equations (1) and (2).

$$B(z) = \frac{\mu_0 NI}{2l(r_o - r_i)} \left[\frac{l}{2-z} \ln \frac{r_o + \sqrt{r_o^2 + \left(\frac{l}{2-z}\right)^2}}{r_i + \sqrt{r_i^2 + \left(\frac{l}{2-z}\right)^2}} + \frac{l}{2+z} \ln \frac{r_o + \sqrt{r_o^2 + \left(\frac{l}{2+z}\right)^2}}{r_i + \sqrt{r_i^2 + \left(\frac{l}{2+z}\right)^2}} \right]. \quad (8)$$

5. Results and Discussions

5.1. Preliminary Studies

The results of the preliminary studies show very clearly that the magnetic properties of the weld differ from the base material. This is due to the change of the microstructure caused by the rapid cooling of the molten material after the RSW-process. Figure 6 shows the comparison of the investigated sample in a cross-sectional view, with an illustration of the pMFT-measurement process. The magnetic field distribution at the sample's surface in a magnetized state with a magnetization current of $I_{\text{mag}} = 35$ A shows very clearly the position of the weld. Therefore, it can be assumed that the magnetic properties differ between the weld and the base material. The true-to-scale overlay confirms this.

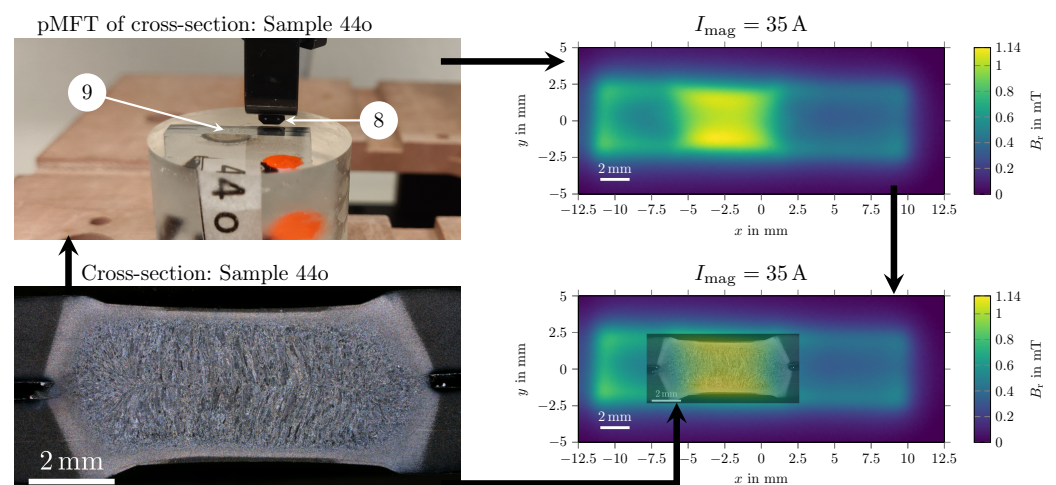


Figure 6. Comparison of the cross-section specimen with clear representation of the weld nugget (**bottom left**). A view of the pMFT-measurement with the Hall-probe (8) and the cross-sectional sample (9) (**top left**), and the results of the flux density measurements after magnetizing the specimens with 35 A (**top right**), and the true-to-scale overlay of the cross-section with the magnetic field distribution (**bottom right**).

The 2D scanning measurements offer the advantage of measuring and visualizing the magnetic field distribution across an area. The evaluation methods developed during the preliminary studies are based on statistical analyses of the region of interest (ROI). Figure 7 shows the results of the investigated magnetized cross-sectional sample. Here, the ROI of the weld is compared with that of the entire sample. The mean values of both ROI rise continuously up to a coil current of $I_{\text{mag}} = 20$ A. As the coil current continues to increase, the values show little change, indicating magnetic saturation of the sample. The respective maximum values of the ROI are the same for each magnetized state. This means that the weld structure has a higher residual magnetic flux density than the surrounding material,

since both ROIs include the weld. The minimum and average values differ from each other. This clearly shows that the magnetic properties of the weld differ from those of the base material. However, in the magnetization of the cross-section samples, the magnetic field lines run through the base material and the weld. No field lines run only through the weld. The following test results show this on the basis of the disc samples. Prior to this, the results on the respective base materials are presented on the basis of toroidal ring specimens.

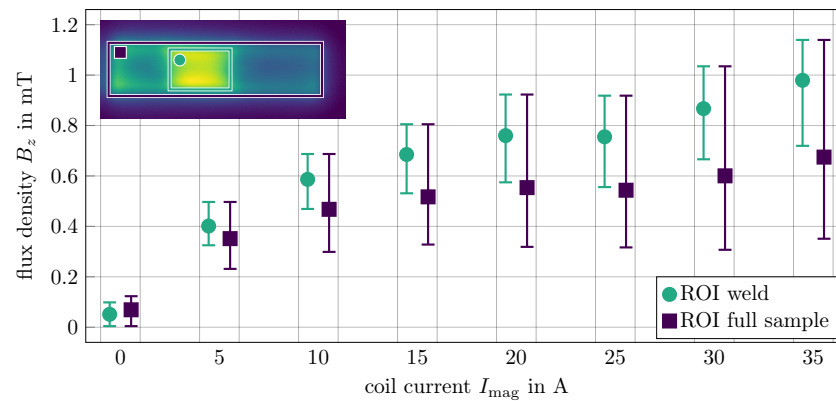


Figure 7. Measurement results of the residual magnetic flux density measurements of the cross-sectional sample with increasing coil current and presentation of the evaluation by means of ROI with the mean, minimum and maximum values therein.

5.2. Hysteresis Loops of the Toroidal Ring Measurements

The results of the toroidal ring measurements as hysteresis loops are shown in Figure 8. It can be clearly seen that the magnetic properties of all materials differ greatly from each other. As expected, MAT3 shows paramagnetic behavior with no evidence of a hysteresis loop. MAT4 shows the lowest coercivity H_c followed by MAT2 and MAT1. This allows us to classify the materials according to DIN EN 60404-1 [12] into the soft magnetic for MAT2 and MAT4, and MAT1 for the hard magnetic materials. The reason for the different coercivity levels can be found in the microstructure on the one hand and in the alloying elements on the other. MAT1 is a quenched and tempered material with a martensitic microstructure, while MAT2 and MAT4 have a ferritic microstructure. Martensitic microstructures usually exhibit higher coercivity than ferritic microstructures, as also reported in [24]. The differences in the MAT2 and MAT4 ferritic materials can be attributed to the alloying elements. MAT2 contains aluminum and titanium, while in MAT4 these elements are not alloyed. Both elements lead to higher coercivity. In addition, the alloying elements lead to a finer microstructure with smaller grain sizes, which also results in higher coercivity [14]. Additionally, the saturation flux density B_s at H_s differs depending on the material. Here, the order is reversed compared to H_c . The characteristic values of the hysteresis loops of each material are listed in Table 7.

Table 7. Characteristic values of the hysteresis loops of the investigated materials.

Material-ID	H_c	H_s	B_s	B_r
MAT1	$\pm 3506 \text{ A m}^{-1}$	$27,490 \text{ A m}^{-1}$	$\pm 1.66 \text{ T}$	$\pm 0.98 \text{ T}$
MAT2	$\pm 904 \text{ A m}^{-1}$	$27,462 \text{ A m}^{-1}$	$\pm 1.95 \text{ T}$	$\pm 1.01 \text{ T}$
MAT3	$\pm 0 \text{ A m}^{-1}$	$27,532 \text{ A m}^{-1}$	–	$\pm 0 \text{ T}$
MAT4	$\pm 246 \text{ A m}^{-1}$	$27,501 \text{ A m}^{-1}$	$\pm 2.07 \text{ T}$	$\pm 1.09 \text{ T}$

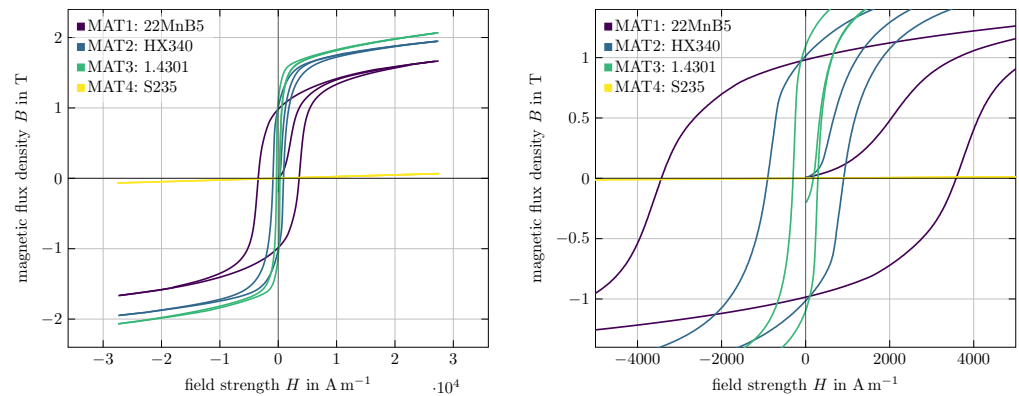


Figure 8. Measurement results of the toroidal rings of the base materials MAT1 to MAT4 in full scale (left) and in detail (right).

5.3. Results of the Vibrating Sample Magnetometer

Figure 9 shows the results of the VSM-measurements. The polarization curves reflect the internal magnetic properties of the material. The saturation range varies between ± 1.5 T and ± 1.8 T. It can be seen that the press-hardening steel 22MnB5 (MAT1) has a higher saturation range than the deep drawing steel HX340LAD (MAT2). A difference of approximately ± 0.3 T can be seen. It is noticeable here that the characteristic loop of a hysteresis curve is not clearly visible. This is not missing, but the curves lie approximately on top of each other. A detailed view demonstrates the dense position of the hysteresis loops in Figure 9 (right). Here, the magnetic properties differ significantly between the base material and weld. The problem in the evaluation of the data lies in the resolution and the discontinuity of the signal. Especially for the base material, no residual magnetic flux density can be analyzed. This might be due to the disadvantage in creating such hysteresis curves with the geometry of the samples used, which is not analytically determinable. The difficulty lies in the fact that the magnetization in a small sample is different at the edge region compared to the interior of the sample. Only an ellipsoid can be analytically determined [14]. Further experiments using the VSM in this context can be found in [2,25].

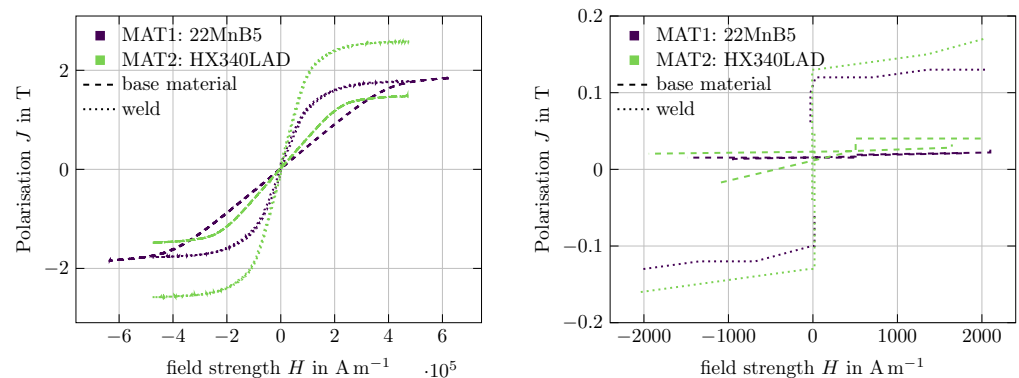


Figure 9. Measurement results of VSM-measurements of the base material and the weld of MAT1 and MAT2 in full scale (left) and in detail (right).

5.4. Measurements of the Residual Magnetic Flux Density

5.4.1. Results of the Sample Preparation and Test Setup Configurations

The measurements by means of VSM already show a different magnetic behavior of base materials and welds. Furthermore, significant differences between the materials MAT1 and MAT2 investigated with the VSM are also evident. Thus, the RMFD-measurements with the disc-samples were carried out for further characterization. As mentioned above, topographic measurements were performed prior to the magnetic measurements to evaluate the geometry of the discs, as shown in Figure 10. The disc thicknesses t were determined

by means of calipers and the evaluation of the topographic measurements on both sides. The flatness of the discs was determined by means of profile sections of the topographic measurements. In this process, 180 radially arranged profile sections with an angular spacing of 1° were generated. From this, the average spherical radius r was calculated using the best-fit circle method from the average profile section of all. The thickness evaluation shows three samples being significant thinner compared to the others. The comparison between both sides and the manually measured thickness are in the same region and can be considered comparable. The spherical radii r are in a size range that is considered negligible in relation to the disc diameters.

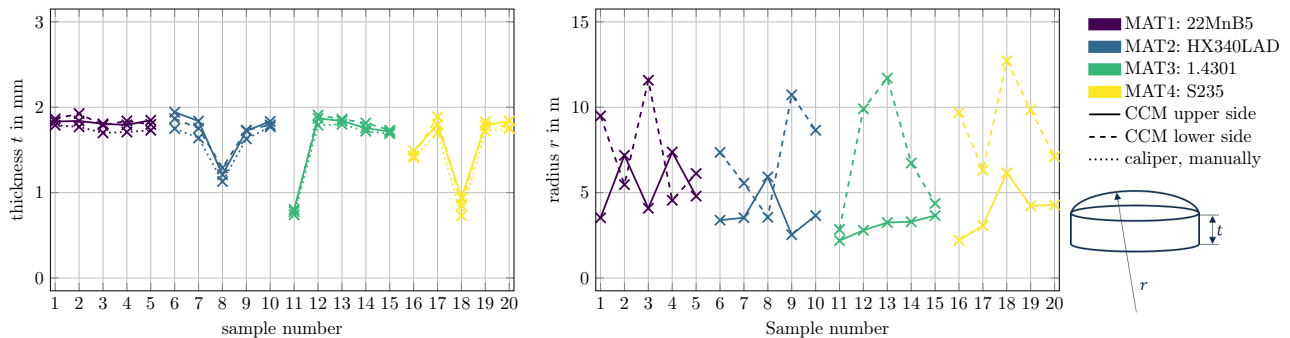


Figure 10. Thickness t of each disc-sample measured by CCM and manually by means of a caliper (left) and spherical radius r to evaluate the surface flatness after the preparation of the samples (right).

The validation measurements to evaluate the generated magnetic fields are shown in Figure 11. Thereby, the measured data from the experiment differ only insignificantly from those of the theoretical consideration according to Equations (1), (2) and (8). As expected, the magnetic field strength H decreases significantly with increasing axial distance z from the center of the coil $z = 0$.

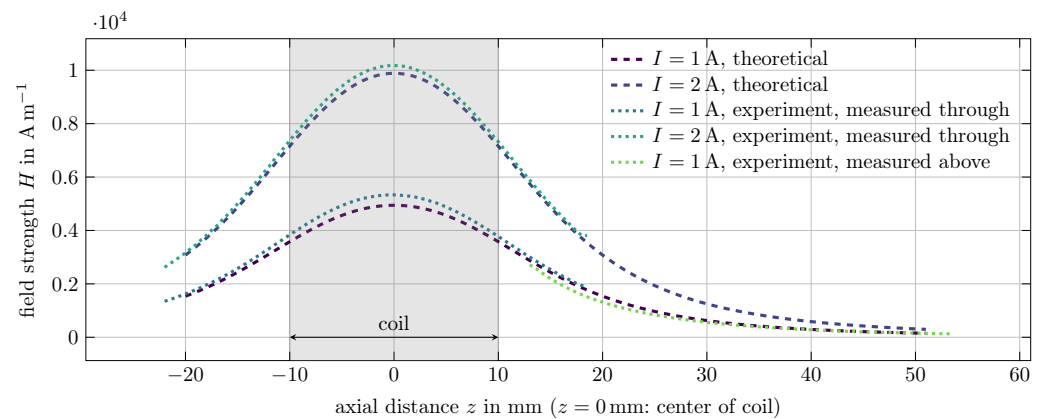


Figure 11. Generated magnetic field at different currents of the magnetization coil with $N = 180$ of enameled copper wire $A_{Cs} = 0.28 \text{ mm}^2$, $d_i = 27 \text{ mm}$, $d_o = 27 \text{ mm}$ and a coil height $h = 20 \text{ mm}$.

5.4.2. Evaluation of the RMFD-Measurements

Figure 12 shows the direct comparison between the microscope and the selected configurations of the measured nuggets d_n . The discs and welds stand out clearly for every RMFD-measurement. Differences lie in the ranges of measurable residual flux density. For the randomly selected sample 20 of MAT4, the difference between microscope and magnetic measurements is less than 0.2 mm. This confirms the good suitability of the selected measurement methods for the magnetic characterization of the weld microstructure.

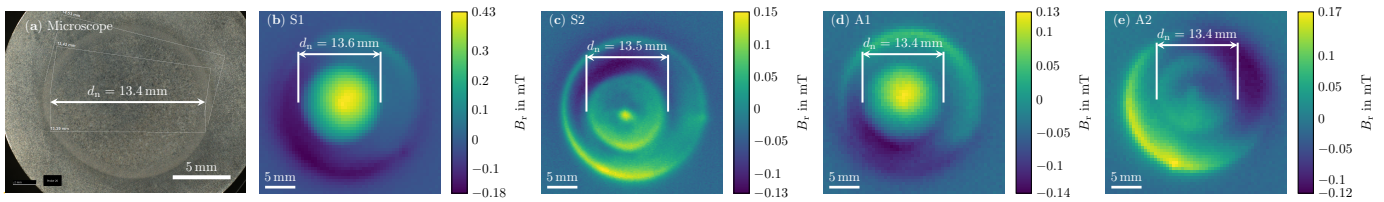


Figure 12. Nugget size d_w determined on microscope (a) compared with flux density measurements in configurations (b) S1, (c) S2, (d) A1, and (e) A2 of magnetized sample 20 of MAT4 ($I_{\text{mag}} = 20$ A).

For the evaluation of the residual magnetic flux density, two ROIs were chosen with an elliptical or circular shape. The ROI-weld contained only the data points of the weld microstructure whereas the ROI-sample contained all data points of the sample including the weld. Subtracting both ROIs from each other yields the third ROI-base-material. Figure 13 shows the selected ROIs on the example of sample 06 of MAT2 in S1-configuration. The evaluation of the ROIs as boxplots shows clearly the difference between the magnetic flux density distribution of the weld, the full sample and the base material. This difference can also be represented by the mean value. Therefore, the mean values of the ROI-weld, ROI-base-material and their difference, named *delta*, were evaluated for the magnetic characterization of the materials.

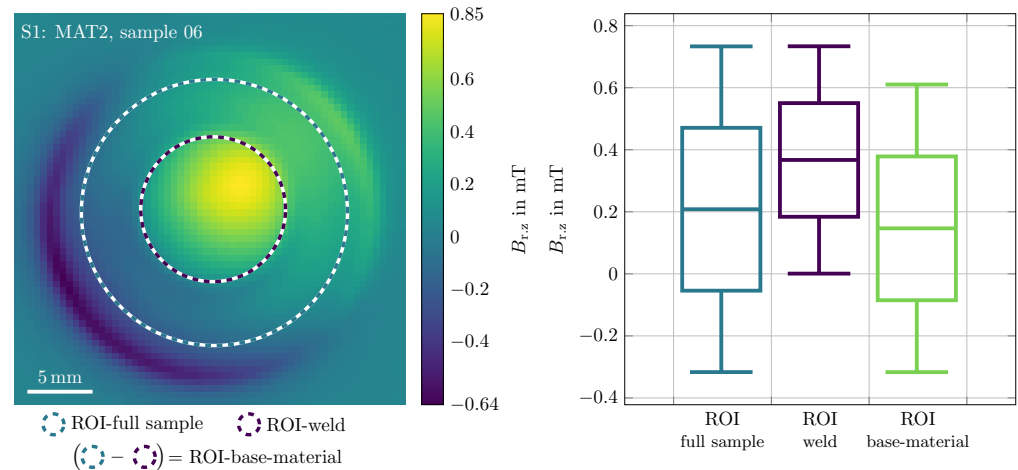


Figure 13. Representation of the ROIs as circular shapes on the example of sample 06 of MAT2 (left) with the comparison of the flux density distribution of the individual ROI as boxplots both ROIs and the difference of them as ROI-base-material (right).

The evaluation of the 2D-surface scans of the residual magnetic flux density in z -direction $B_{r,z}$ is shown in Figure 14. From left to right, it shows the measurement data at increasing coil currents I_{mag} for the weld and base material regions and the difference named *delta* between them for the configurations and materials investigated.

The mean values were calculated over all five disc-samples per material at each coil current stage. The standard deviation turns out to be relatively small. It increases with decreasing flux density, which indicates a poorer signal-to-noise ratio. All diagrams show that the materials differ from each other in their magnetic behavior in the same way as already observed in the toroidal ring core measurements of Section 5.2. MAT1 shows the highest flux densities of all materials. MAT4 has the lowest residual flux density in the group of ferromagnetic materials at any parameter setting. MAT2 lies between MAT1 and MAT4. A different behavior between the weld microstructure and the base material can also be observed. In general, the measurable magnetic flux densities of the weld structures are higher than those of the base materials are. The base materials of MAT2 and MAT4 hardly exhibit any residual magnetization, which is actually only to be expected for MAT3.

The difference plots *delta* (Figure 14c,f,i,l) clearly highlight the differences between the weld-structures and the base materials.

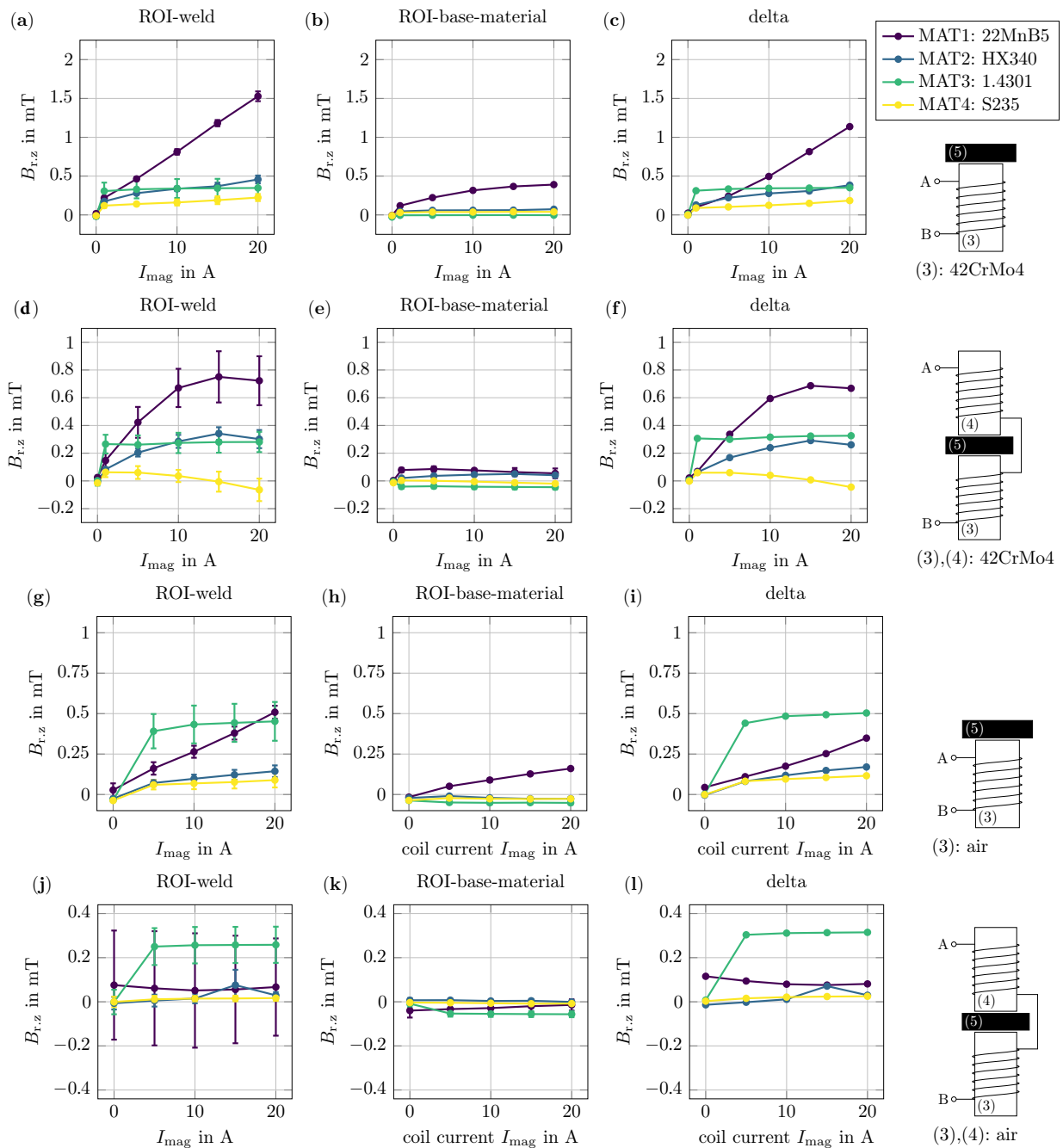


Figure 14. Mean values and standard deviations of the residual magnetic flux density in z-direction $B_{r,z}$ of the ROIs weld (left), base material (center), and the difference of both ROIs *delta* (right) for all configurations: S1 (a–c), S2 (d–f), A1 (g–i) and A2 (j–l) over increasing coil currents I_{mag} . The mean values are calculated over the five discs per material at each coil current level I_{mag} .

It is noticeable that the highest residual flux densities were measured for coil configuration S1, followed by S2, A1 and A2, when comparing the individual coil-configurations with each other. Coil configuration A2 shows the lowest residual magnetic flux densities for the ferromagnetic materials. The standard deviations are very large in this configuration for the ROI-weld. This indicates that this configuration is not suitable for these materials. S1 and A1 show similar behavior, although only about half as high residual flux density

values can be achieved with the coil configuration A1. While MAT2, MAT3, and MAT4 exhibit saturation behavior is already at $I_{\text{mag}} = 5$ A, this behavior could not be observed for MAT1. The measured flux density increases linearly without a change of the gradient in the investigated range of the magnetizing current up to $I_{\text{mag}} = 20$ A. In contrast to this, the region of the base material shows saturation behavior. Figure 15 highlights this as 2D-surface scans for each individual coil current stage for sample 05 in the A1-configuration.

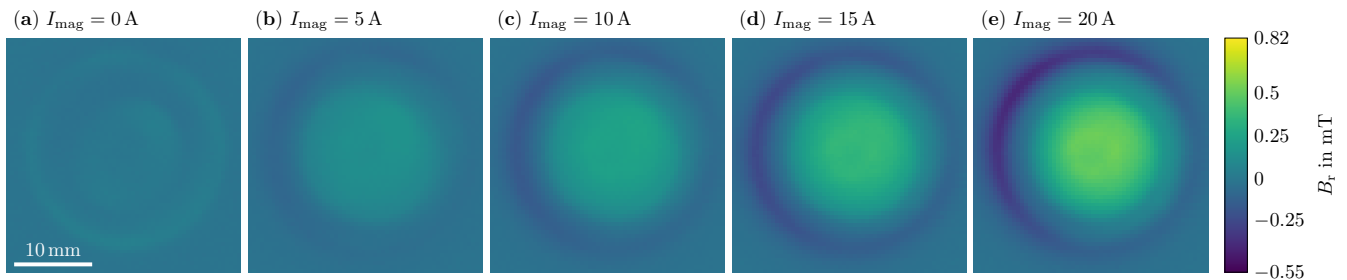


Figure 15. Two dimensional (2D)-surface scans of the residual magnetic flux density of sample 05 of MAT1 with increasing coil currents I_{mag} in A1-configuration.

The base material of MAT3 exhibits the usual paramagnetic behavior. In contrast, the weld-microstructure shows a clearly measurable residual flux density over the entire nugget-microstructure already at $I_{\text{mag}} = 1$ A. This does not increase much further even with larger magnetization fields as visualized in Figure 16. This relationship applies for all coil configurations. As a result, the choice of the coil configuration has little effect on the achievable residual flux density, whereby a $B_{r,z} = 0.1$ mT lower residual flux density is obtained when using the steel core ($\bar{B}_{r,z} = 0.34$ mT) compared to the air core coil ($\bar{B}_{r,z} = 0.44$ mT). It can be assumed that no higher flux density values can be expected with other configurations. These results confirm the good suitability of pMFT for NDT of spot welds of material MAT3 as already demonstrated in [9].

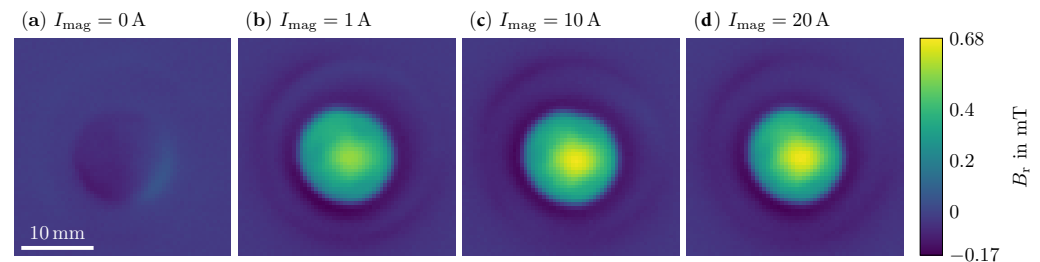


Figure 16. Two dimensional (2D)-surface scans of the residual magnetic flux density of sample 14 of MAT3 with increasing coil currents I_{mag} in S1-configuration.

Coil configuration S2 shows unexpected behavior for the three ferromagnetic materials. The achieved residual flux density decreases slightly at coil currents of $I_{\text{mag}} = 15$ A and above. For MAT4, this phenomenon even leads to a reversal of the magnetic field direction. The reason for this has not been investigated yet. A first assumption is the increasing magnetic attraction of the coils to each other. This leads to mechanical impact on the samples during the magnetization process. Nevertheless, this has not been proven yet. It is noticeable that, in the direct comparison of A1 and S2, the achieved residual flux densities are in a similar magnitude range. For MAT1, the linear increase cannot be observed in the S2-configuration. The direct comparison of the 2D-surface scans in Figure 17 for MAT4, sample 19 are interesting. It seems that with S2 the individual structures of the spot weld including the HAZ can be represented at higher magnetization currents, which is reflected in individual rings. This can be attributed to the different microstructural properties, according to which different hardness values correlate with the magnetic behavior. In [26], it was shown that the hardness is inversely proportional to the residual flux density

achieved, while in [27], H_c is directly proportional to the hardness for ultra-high strength steel as MAT1.

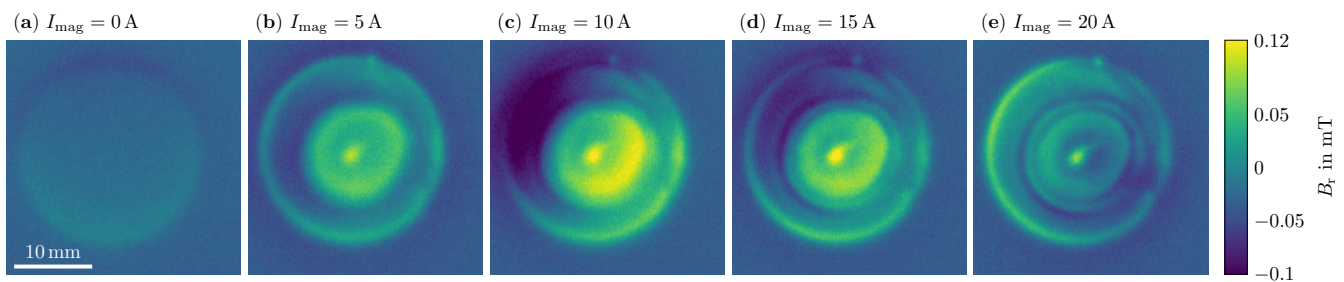


Figure 17. Two dimensional (2D)-surface scans of the residual magnetic flux density of sample 19 of MAT4 with increasing coil currents I_{mag} of S2-configuration with the appearance of rings at higher magnetic flux densities.

6. Conclusions

Based on the hypothesis that the test results of the pMFT-method are influenced by the microstructure of the nugget of a spot welded joint, various measurement methods were investigated to characterize the magnetic behavior of the microstructures of the weld and the base material. The different test methods used to determine the magnetic properties of the materials investigated show differing suitabilities.

The preliminary investigations on conventional cross-section specimens showed that the magnetic properties of the microstructures of the two regions differ from each other. Based on these results, hysteresis loops were determined with ring core samples of the base materials in order to classify them magnetically. Accordingly, the materials were divided into ferromagnetic and paramagnetic, and the ferromagnetic materials into soft and hard magnetic ones.

For the examination of small volumes such as spot-weld nuggets, the VSM-method seemed to be very suitable for characterizing the regions of the welds magnetically. Subsequently, small samples were cut out of the spot welds and of the base material. However, based on the measurement results, it is difficult to precisely determine the residual flux density.

Since the measurements on the cross-section samples already provided purposeful results, this method was further investigated. In the case of the cross-section specimens, there are no regions in which the magnetic flux passes only through the structure of the nugget. It is always a mixture of base material and weld. Furthermore, the magnetization direction is not the same as in the pMFT-method. Therefore, specimen discs were cut out of the center sheet of spot-welded triple-sheet joints and prepared for the residual flux density measurements. This preparation of the specimens ensures the exposure of the different zones of the welded joint as separate and homogeneous volumes. Thus, based on the pMFT-method, 2D-surface scans with different magnetization states could be performed on the sample surfaces. It was shown that the geometry of the nugget can be determined in the magnetic measurements by comparing them to microscope images of the nuggets. This gain in knowledge alone already shows that the magnetic properties must be different between the weld structure and the base material. In further investigations with four different magnetization configurations, the characteristic differences of the four materials could be demonstrated. It was shown in detail that the four configurations influence the measurable residual magnetic flux density. The highest densities on the sample disc surfaces were achieved with the one-sided variant with a steel core. This variant should be preferred in future investigations. Lower residual flux density values were measured with magnetization on both sides and a steel core. This configuration may provide more detailed results with regard to the different microstructural zones of the welded joint. The evaluation method by means of ROI shows a possible variant, which can be applied for further investigations on similar samples. These can be, among others, the NDT of materials to detect inhomogeneities such as cracks, voids, inclusions without mechanical

contact. This should be examined in more detail in future studies, e.g., with hardness measurements and comparisons under an optical microscope.

In general, the measurement on toroidal samples is to be preferred, since closed magnetic circuits are used. The other two test methods, VSM and RMFD, both use open magnetic circuits. The different materials show the same trends in all methods. The determined residual magnetic flux density values of the hysteresis loops from the ring core samples of MAT1, MAT2 and MAT4 are in the range of $B_r = 1$ T. They cannot be measured with the other two methods, where almost no residual flux density can be measured for the base materials. This shows that a comparability is only possible within one method. It is necessary to examine the extent to which toroidal core samples can be prepared out of RSW-nuggets. Thus, measurements of hysteresis loops and Rayleigh loops of the welded structure can be performed to investigate physical relationships in the future.

Based on these investigations, the pMFT-method for NDT of spot welds can be further developed. In the future, the results are to be implemented in numerical models for the simulation of the measuring principle. In this way, the understanding of the physical effect of the test method can be deepened.

Author Contributions: Conceptualization, C.M.; methodology, C.M.; software, C.M.; validation, C.M. and E.Z.; formal analysis, C.M.; investigation, C.M., E.Z. and A.R.; resources, C.M.; data curation, C.M.; writing—original draft preparation, C.M.; writing—review and editing, C.M., J.K. and J.Z.; visualization, C.M.; supervision, U.F.; project administration, C.M., J.K., J.Z. and U.F.; funding acquisition, C.M., J.K., J.Z. and U.F. All authors have read and agreed to the published version of the manuscript.

Funding: The research project IFG 21.542BR/DVS 04.3321 “Non-destructive testing of projection welded joints on sheet metal structures” from the Research Association DVS—Deutscher Verband für Schweißen und verwandte Verfahren e. V. of the German Welding Society, Aachener Str. 172, 40223 Düsseldorf, is supported by the Federal Ministry of Economic Affairs and Climate Action the German Federation of Industrial Research Associations (AiF) as part of the program for promoting industrial cooperative research (IGF) on the basis of a decision by the German Bundestag. The project is carried out at Technische Universität Dresden, Chair of Joining Technology and Assembly.

Institutional Review Board Statement: Not applicable.

Informed Consent Statement: Not applicable.

Data Availability Statement: Not applicable.

Acknowledgments: The authors would like to thank the members of the project advisory committee, our students, and all other contributors for their support during the research project IFG 21.542BR/DVS 04.3321 “Non-destructive testing of projection welded joints on sheet metal structures”.

Conflicts of Interest: The authors declare no conflict of interest.

Abbreviations

The following abbreviations are used in this manuscript:

CCM	chromatic-confocal microscope
EDM	electrical discharge machining
RSW	Resistance spot welding
HAZ	heat-affected zone
NDT	non-destructive testing
pMFT	passive magnetic flux density testing
RMFD	residual magnetic flux density
ROI	region of interest
VSM	vibrating sample magnetometer

Nomenclature

A_{cs}	cross-sectional area (mm ²)
B	flux density (T)
B_r	residual magnetic flux density (T)
B_s	flux density at saturation (T)
d	diameter (mm)
$d_{eu/el}$	indentation diameter (mm)
d_n	nugget diameter (mm)
d_i	inner diameter (mm)
d_o	outer diameter (mm)
d_w	weld diameter (mm)
$e_{u/l}$	electrode indentation (mm)
e_{max}	limit of electrode indentation (mm)
f	frequency (Hz)
F_{el}	electrode force (kN)
H	magnetic field strength (A m ⁻¹)
H_c	magnetic coercivity (A m ⁻¹)
H_s	magnetic field strength at saturation (A m ⁻¹)
h	height (mm)
I_{mag}	magnetization current (A)
I_w	welding current (kA)
l_m	average length (mm)
N_i	number of coil windings
r	radius (mm)
t	sheet thickness (mm)
t_w	weld time (s)
U_{ind}	induced voltage (V)
U_{mag}	magnetization voltage (V)
α_R	Rayleigh-constant
μ	permeability H m ⁻¹
μ_0	vacuum permeability H m ⁻¹
μ_r	relative permeability

References

1. DVS 2916-5:2017-5; Prüfen von Widerstandspressschweißverbindungen: Zerstörungsfreie Prüfung. DVS Media GmbH: Düsseldorf, Germany, 2017.
2. Füssel, U.; Mathiszik, C.; Zschetzsche, J.; Großmann, C.; Heide, M. *Zerstörungsfreie Bewertung des Linsendurchmessers Beim Widerstandspunktschweißen Mit Magnetischen Prüfverfahren*; Technische Universität Dresden, Professur für Fügetechnik und Montage: Dresden, Germany, 2015. [[CrossRef](#)]
3. Mathiszik, C.; Füssel, U.; Zschetzsche, J. *Zerstörungsfreie Bewertung des Linsendurchmessers beim Widerstandspunktschweißen durch bildgebende Analyse der Remanenzflussdichte*; DVS Berichte: Sondertagung Widerstandsschweißen 2016 in Duisburg; DVS Media GmbH: Düsseldorf, Germany, 2016.
4. Mathiszik, C.; Zschetzsche, J.; Großmann, C.; Füssel, U. Remanent Magnetization for Non-Destructive Testing of Spot Welds. In Proceedings of the 19th WCNDT 2016—World Conference on Non-Destructive Testing, Munich, Germany, 13–17 June 2016. [[CrossRef](#)]
5. Füssel, U.; Mathiszik, C.; Zschetzsche, J. *Zerstörungsfreie Charakterisierung der Anbindungsfläche beim Widerstandspressschweißen Durch Bildgebende Analyse der Remanenzflussdichte*; Technische Universität Dresden, Professur für Fügetechnik und Montage: Dresden, Germany, 2019.
6. Mathiszik, C.; Zschetzsche, J.; Füssel, U. Automated non-destructive evaluation of spot welds using the imaging analyses of the residual magnetic flux density. In Proceedings of the ASNT Research Symposium 2019, Stanford, CA, USA, 10–12 September 2019.
7. Mathiszik, C.; Reinhardt, T.; Zschetzsche, J.; Füssel, U. NDT of spot welds by imaging analysis of the residual magnetic flux density—Investigation on the influence of electrode indentation on the measurement results. *Mater. Test.* **2018**, *60*, 1179–1183. [[CrossRef](#)]
8. ISO 14373:2015-06; Widerstandsschweißen—Verfahren zum Punktschweißen von Niedriglegierten Stählen Mit oder Ohne Metallischem Überzug. DIN Deutsches Institut für Normung e. V. Beuth Verlag GmbH: Berlin, Germany, 2015. [[CrossRef](#)]

9. Mathisizik, C.; Reinhardt, T.; Zschetzsche, J.; Füssel, U. NDT of austenitic steels—Evaluation of spot weld nugget diameters by imaging analyses of the residual flux density. In Proceedings of the 12th ECNDT, ECNDT and European Federation for Non-Destructive Testing and European Conference on Non-Destructive Testing, Sweden MEETX AB, Gothenburg, Sweden, 11–15 June 2018; Volume ECNDT2018.
10. Holleman, A.F.; Wiberg, E.; Wiberg, N. *Lehrbuch der Anorganischen Chemie*, 101st ed.; de Gruyter: Berlin, Germany, 1995.
11. Bramerdorfer, G.; Kitzberger, M.; Wöckinger, D.; Koprivica, B.; Zurek, S. State-of-the-art and future trends in soft magnetic materials characterization with focus on electric machine design—Part 2. *Tech. Mess.* **2019**, *86*, 553–565. [[CrossRef](#)]
12. *DIN EN 60404-1:2017-08*; Magnetic Materials—Part 1: Classification. DIN Deutsches Institut für Normung e. V. Beuth Verlag GmbH: Berlin, Germany, 2017. [[CrossRef](#)]
13. Tumanski, S. *Handbook of Magnetic Measurements*, 1st ed.; Series in Sensors; CRC Press: Boca Raton, FL, USA, 2016.
14. Kneller, E.; Seeger, A.; Kronmüller, H. *Ferromagnetismus*; Springer: Berlin/Heidelberg, Germany, 1962. [[CrossRef](#)]
15. Lord Rayleigh, S.S.R. XVII. On the maintenance of vibrations by forces of double frequency, and on the propagation of waves through a medium endowed with a periodic structure. *Lond. Edinb. Dublin Philos. Mag. J. Sci.* **1887**, *24*, 145–159. [[CrossRef](#)]
16. *DIN EN 60404-4:2009-08*; Magnetic Materials—Part 4: Methods of Measurement of d.c. Magnetic Properties of Magnetically Soft Materials. DIN Deutsches Institut für Normung e. V. Beuth Verlag GmbH: Berlin, Germany, 2009. [[CrossRef](#)]
17. Mathis, W.; Reibiger, A. *Küpfmüller Theoretische Elektrotechnik*; Springer: Berlin/Heidelberg, Germany, 2017. [[CrossRef](#)]
18. Chang, L.; Jahns, T.M.; Blissenbach, R. Characterization and Modeling of Soft Magnetic Materials for Improved Estimation of PWM-Induced Iron Loss. *IEEE Trans. Ind. Appl.* **2020**, *56*, 287–300. [[CrossRef](#)]
19. *DIN EN 60404-2:2009-01*; Magnetic Materials—Part 2: Methods of Measurement of the Magnetic Properties of Electrical Steel Strip and Sheet by Means of an Epstein Frame. DIN Deutsches Institut für Normung e. V. Beuth Verlag GmbH: Berlin, Germany, 2009. [[CrossRef](#)]
20. Takahashi, S.; Kobayashi, S.; Kikuchi, H.; Kamada, Y.; Ara, K. Analysis of Minor Hysteresis Loops of Cold Rolled Low Carbon Steel. *IEEE Trans. Magn.* **2006**, *42*, 3782–3784. [[CrossRef](#)]
21. Mathisizik, C.; Köberlin, D.; Heilmann, S.; Zschetzsche, J.; Füssel, U. General Approach for Inline Electrode Wear Monitoring at Resistance Spot Welding. *Processes* **2021**, *9*, 685. [[CrossRef](#)]
22. Duffy, R.M.; Netterfield, R.P. Design of Faraday rotators and modulators. *Rev. Sci. Instrum.* **1984**, *55*, 743–746. [[CrossRef](#)]
23. Basharat, M.; Ding, M.; Cai, H.; Li, Y.; Fang, J.; Liu, P.; Tu, X. Design and Analysis of Multilayer Solenoid Coil for Faraday Modulator. *Matec Web Conf.* **2017**, *114*, 04004. [[CrossRef](#)]
24. Hünicke, U.D.; Möller, S. Auswertung der statischen Magnetisierungskurve zur Kontrolle von Gefüge- und Behandlungszuständen bei Stählen. In *Proceedings of the ZfP in Forschung, Entwicklung und Anwendung*, [Elektronische Ressource] ed.; DGZfP, Ed.; Jahrestagung Zerstörungsfreie Materialprüfung and Deutsche Gesellschaft für Zerstörungsfreie Prüfung, DGZfP: Mainz, Germany, 2003; Volume 83-CD.
25. Vinz, J. Simulation der Remanenzflussdichte Mittels der Finiten-Elemente-Methode. Diploma Thesis, Technische Universität Dresden, Dresden, Germany, 2016.
26. Ankener, W.; Böttger, D.; Smaga, M.; Gabi, Y.; Strass, B.; Wolter, B.; Beck, T. Micromagnetic and Microstructural Characterization of Ferromagnetic Steels in Different Heat Treatment Conditions. *Sensors* **2022**, *22*, 4428. [[CrossRef](#)]
27. Zhang, Y.; Wang, Z.J.; Wang, Y.L.; Zhang, Z.J.; Zhang, Y.S. A Study on the Relationship between Hardness and Magnetic Properties of Ultra-High Strength Steel. *Adv. Mater. Res.* **2014**, *1063*, 78–81. [[CrossRef](#)]